THE JOURNAL OF NAVIGATION (2019), **72**, 741–758.
doi:10.1017/S037346331800084X

Error Modelling and Optimal Estimation of Laser Scanning Aided Inertial Navigation System in GNSS-Denied Environments

W.I. Liu[1,2], Zhixiong Li[3,4] and Zhichao Zhang[1]

[1](*School of Mechanical and Electrical Engineering, China University of Mining and Technology, Xuzhou 221116, China*)
[2](*Jiangsu Key Laboratory of Mine Mechanical and Electrical Equipment, China University of Mining & Technology, Xuzhou 221116, China*)
[3](*Department of Marine Engineering, School of Engineering, Ocean University of China, Qingdao 266100, China*)
[4](*School of Mechanical, Materials, Mechatronic and Biomedical Engineering, University of Wollongong, Wollongong, NSW 2522, Australia*)
(E-mail: zhixiong.li@ieee.org)

A Laser Scanning aided Inertial Navigation System (LSINS) is able to provide highly accurate position and attitude information by aggregating laser scanning and inertial measurements under the assumption that the rigid transformation between sensors is known. However, a LSINS is inevitably subject to biased estimation and filtering divergence errors due to inconsistent state estimations between the inertial measurement unit and the laser scanner. To bridge this gap, this paper presents a novel integration algorithm for LSINS to reduce the inconsistences between different sensors. In this new integration algorithm, the Radial Basis Function Neural Networks (RBFNN) and Singular Value Decomposition Unscented Kalman Filter (SVDUKF) are used together to avoid inconsistent state estimations. Optimal error estimation in the LSINS integration process is achieved to reduce the biased estimation and filtering divergence errors through the error state and measurement error model built by the proposed method. Experimental tests were conducted to evaluate the navigation performance of the proposed method in Global Navigation Satellite System (GNSS)-denied environments. The navigation results demonstrate that the relationship between the laser scanner coordinates and the inertial sensor coordinates can be established to reduce sensor measurement inconsistencies, and LSINS position accuracy can be improved by 23·6% using the proposed integration method compared with the popular Extended Kalman Filter (EKF) algorithm.

KEYWORDS

1. Laser Scanning Aided Inertial Navigation. 2. Autonomous Navigation. 3. GNSS-Denied Environment. 4. Singular Value Decomposition Unscented Kalman Filter.

Submitted: 6 January 2017. Accepted: 27 September 2018. First published online: 15 November 2018.

1. INTRODUCTION. Autonomous navigation has attracted considerable attention in the indoor, underground mining, subway, railway, underwater and tunnel industries. However, Global Navigation Satellite System (GNSS) signals are not always available in these areas (Hesch et al., 2016; Allotta, et al., 2014). In order to estimate the positions of moving objects in GNSS-denied environments, it is necessary to use other sensors to measure the displacements of the moving objects. For this reason, an Inertial Measurement Unit (IMU) that senses three Degrees Of Freedom (DOF) linear accelerations as well as three DOF rotational velocities of a moving object has been widely used in attitude measurement. However, IMU measurements are often corrupted by background noise, and the consequent biased estimation and filtering divergence errors will result in unreliable position and attitude estimation during autonomous navigation (Allotta et al., 2012). Furthermore, due to drift over time, an IMU will accumulate measurement errors (Wang et al., 2015; Markham et al., 2012). Although an IMU's drift can be bounded within an acceptable arrange to improve measurement accuracy, IMUs are generally too expensive for practical everyday use (Lehtola et al., 2016). For practical applications, some alternative sensors, such as Light Direction And Ranging (LiDAR), laser scanning or cameras, have been applied to calculate the position and attitude of moving objects in GNSS-denied environments. As a laser scanner can provide both the distance and azimuth information for IMUs with high accuracy and efficiency, it has been commonly utilised in moving object navigation (Lauterbach et al., 2015; Bosse et al., 2012).

Recent work has demonstrated that a Laser Scanning aided Inertial Navigation System (LSINS) can obtain highly accurate position and attitude information for moving object navigation. This combination of laser scanning and inertial measurements assumes prior knowledge on the rigid transformation between different sensors (Soloviev and Uijt De Haag, 2010; Tang et al., 2015; Shi et al., 2015). However, inconsistencies are usually found between laser scanning and inertial measurements, and hence the combination has not delivered satisfactory results in existing LSINS. Biased estimation and filtering divergence errors are consequently generated and decrease the navigation accuracy (Xiong et al., 2009; Liu et al., 2013; Kim et al., 2012). For example, Hesch et al. (2016) presented an Extended Kalman Filter (EKF) to fuse information from an IMU and a Two-Dimension (2D) laser scanner to concurrently estimate the six DOF position and attitude of a moving object with respect to a Three-Dimension (3D) map of the environment. However, without bias correction, the IMU measurement accumulated attitude estimation errors until divergence. Aghili and Su (2016) achieved a robust six DOF relative navigation solution by combining an Iterative Closest Point (ICP) registration algorithm and a noise Adaptive Kalman Filter (AKF) in a closed-loop configuration. The measurements from a laser scanner and an IMU were processed by the ICP-AKF method in autonomous navigation. Although the proposed ICP-AKF was sensitive to local minima and outliers in the sensory measurements, without proper initial attitude information, the method converged slowly and then diverged. Baglietto et al. (2011) developed a system for mapping and self-localisation based on a six DOF IMU and a laser scanner. The sensory measurements were fed into an Unscented Kalman Filter (UKF)-based Simultaneous Localisation And Mapping (SLAM) algorithm, and experimental results shown that the UKF-based approach failed to integrate multi-sensory data for position estimation.

Literature review indicates that EKF, AKF or UKF algorithms used for LSINS in GNSS-denied environments (Wu et al., 2014; Kong et al., 2016; Sun et al., 2015) can suffer from inconsistencies between different sensors. That is, the error model of LSINS will greatly influence the inconsistent state estimation results, and consequently accumulate biased estimation and filtering divergence errors. Therefore, *a priori* knowledge about the error model of LSINS is required to eliminate state estimation inconsistencies. In the course

https://doi.org/10.1017/S037346331800084X Published online by Cambridge University Press

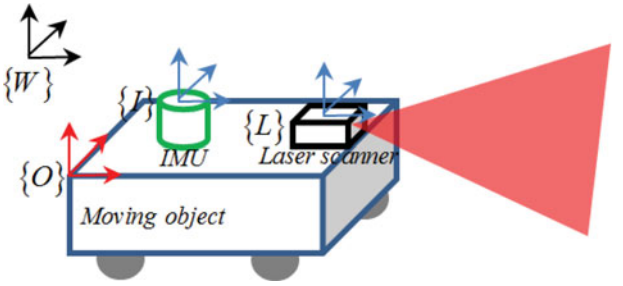

Figure 1. Coordinate frames {*L*}, {*I*}, {*O*} and {*W*} of LSINS.

of LSINS state estimation, the EKF or UKF-based integration algorithms cannot solve the filtering divergence, which may directly affect the measuring accuracy of LSINS (Tan et al., 2015; Chen et al., 2015). Although recent research attempted to control the filter error using a Singular Value Decomposition Unscented Kalman Filter (SVDUKF), singular value decomposition only improves the stability of the state covariance matrix of the UKF algorithm while the state estimation bias caused by measurement uncertainty remains unsolved (Gao et al., 2010). Fortunately, Radial Basis Function Neural Networks (RBFNN) are able to model arbitrary nonlinear dynamic systems and identify system uncertainty (Deng and Zhang, 2013; Jwo and Huang, 2004; Ma et al., 2018; Zhan and Wan, 2006). It is possible to utilise RBFNN to discover the state estimation bias in SVDUKF processing to reduce the biased estimation and filtering divergence errors. However, RBF improved SVDUKF has not yet been investigated in autonomous navigation.

In order to bridge the aforementioned research gap in autonomous navigation, this paper proposes a novel RBF-improved SVDUKF to reduce the biased estimation and filtering divergence errors in the process of LSINS integration. First, the relationship between laser scanner coordinates and inertial sensor coordinates is established to build the error state vector and measurement error model of LSINS. Second, a RBFNN is employed to optimise the model parameters of SVDUKF to improve LSINS position accuracy. In addition, instead of unscented transformation, a RBFNN algorithm can be used to reduce SVDUKF and will be adopted to suppress negative definite variation in the *a priori* covariance matrix of UKF. Lastly, experimental tests are implemented to demonstrate the effectiveness of the proposed method in GNSS-denied environments.

The remainder of this paper is organised as follows. Section 2 describes the error model of LSINS. The proposed error control approach, RBF-improved SVDUKF, is presented in Section 3. An evaluation of the proposed error control method using experimental tests is presented in Section 4 and Section 5 concludes the paper.

2. ERROR MODELLING OF LSINS.

Generally, an LSINS contains four basic coordinate frames: the laser scanner frame {*L*}, the inertial measurement unit frame {*I*}, the object frame {*O*} and the world frame {*W*}. Figure 1 depicts the relationships of these four frames.

2.1. *Transformation between {L} frame and {I} frame.*

To effectively integrate the measurements of the laser scanner and IMU, we should first calculate the relative positions and orientations between these sensors.

https://doi.org/10.1017/S037346331800084X Published online by Cambridge University Press

Assuming that the point ${}^{W}P$ in the $\{W\}$ frame corresponds to the point ${}^{L}P$ in the $\{L\}$ frame, the relationship between the $\{W\}$ and $\{L\}$ frames can be calculated as (Liu, 2017):

$$ {}^{L}P = R_{W}^{L}\,{}^{W}P + {}^{L}T_{LW} \tag{1} $$

where R_{W}^{L} represents a 3×3 orthonormal rotation matrix between the $\{W\}$ and $\{L\}$ frames; ${}^{L}T_{LW}$ is the translation vector. The success of the coordinate transformation depends on finding a suitable R_{W}^{L} and ${}^{L}T_{LW}$.

In order to calculate R_{W}^{L} and ${}^{L}T_{LW}$, the coordinate transformation can be obtained by observing the laser scanning to the calibration plane. A geometric constraint is calculated between the laser scanning points and the calibration planes. As the laser scanning point clouds lie on the calibrating planes, we have:

$$ {}^{W}r \cdot {}^{W}P = d \tag{2} $$

where ${}^{W}r$ denotes the normal vector to the plane and d represents the distance between the $\{W\}$ frame and calibrating plane. Equation (1) can be re-written as:

$$ {}^{W}P = \left(R_{W}^{L}\right)^{-1}\left({}^{L}P - {}^{L}T_{LW}\right) \tag{3} $$

Substituting Equation (3) into Equation (2) yields:

$$ {}^{W}r \cdot \left(R_{W}^{L}\right)^{-1}\left({}^{L}P - {}^{L}T_{LW}\right) = d \tag{4} $$

For a given laser scanning point and a calibration plane position, R_{W}^{L} and ${}^{L}T_{LW}$ have to satisfy the constraint in Equation (4), which can be solved by the following steps.

Step 1: Linear solution. Let us assume that in the $\{L\}$ frame, the coordinates of the laser scanning point can be defined as ${}^{L}P = [{}^{L}P_{x}\ {}^{L}P_{y}\ 0]^{T}$. Therefore, Equation (4) can be rewritten as:

$$ {}^{W}r \cdot \left(R_{W}^{L}\right)^{-1}\left(\begin{bmatrix} {}^{L}P_{x} \\ {}^{L}P_{y} \\ 0 \end{bmatrix} - {}^{L}T_{LW}\right) = {}^{W}r \cdot \left(R_{W}^{L}\right)^{-1}\begin{bmatrix} 1 & 0 & 0 \\ 0 & 1 & -{}^{L}T_{LW} \\ 0 & 0 & 0 \end{bmatrix}\begin{bmatrix} {}^{L}P_{x} \\ {}^{L}P_{y} \\ 1 \end{bmatrix} = d \tag{5} $$

Define $Z = (R_{W}^{L})^{-1}\begin{bmatrix} 1 & 0 & 0 \\ 0 & 1 & -{}^{L}T_{LW} \\ 0 & 0 & 0 \end{bmatrix}$, then Equation (5) can be simplified as:

$$ {}^{W}r \cdot Z \cdot {}^{L}P = d \tag{6} $$

where Z denotes the parameters to be calculated, that is, the unknown R_{W}^{L} and ${}^{L}T_{LW}$. The Least Squares (LS) method is adopted to estimate Z in this paper.

To obtain the optimal estimation of Z, multiple calibration planes are used in the coordinate transformation process. It is assumed that the total numbers of calibration planes are N, and the i-th plane ${}^{W}r_{i} = [r_{i,1}\ r_{i,2}\ r_{i,3}]$ contains $M_{i}(i = 1, \ldots, N)$ laser scanning points. Let us define $Z = \begin{bmatrix} z_{11} & z_{12} & z_{13} \\ z_{21} & z_{22} & z_{23} \\ z_{31} & z_{32} & z_{33} \end{bmatrix}$ for ${}^{W}r_{i}$, the distance between ${}^{W}r_{i}$ and the $\{W\}$ frame

https://doi.org/10.1017/S037346331800084X Published online by Cambridge University Press

origin d_i, and the j-th ($j = 1, 2, \ldots, M_i$) laser scanning point in ${}^{W}r_i\,{}^{L}P_{ij} = [{}^{L}P_{ij,x}\ {}^{L}P_{ij,y}\ 1]^T$. Equation (6) can be then rewritten as:

$$\begin{aligned}(r_{i,1}z_{11} + r_{i,2}z_{21} + r_{i,3}z_{31}) \cdot {}^{L}P_{ij,x} + (r_{i,1}z_{12} + r_{i,2}z_{22} + r_{i,3}z_{32}) \\ \cdot {}^{L}P_{ij,y} + (r_{i,1}z_{13} + r_{i,2}z_{23} + r_{i,3}z_{33}) = d_i\end{aligned} \tag{7}$$

As can be seen in Equation (7), each laser scanning point can be described as a linear equation, and hence, the LS method can be applied to solve Z from the equations. R_W^L and ${}^{L}T_{LW}$ can be then calculated from Z.

Let R_i be the i-th row of R_W^L, then $(R_W^L)^{-1} = (R_W^L)^T = [R_1^T\ R_2^T\ R_3^T]$, and we can obtain:

$$Z = [R_1^T \quad R_2^T \quad R_3^T] \begin{bmatrix} 1 & 0 & 0 \\ 0 & 1 & -{}^{L}T_{LW} \\ 0 & 0 & 0 \end{bmatrix} = [R_1^T \quad R_2^T \quad -(R_W^L)^T\,{}^{L}T_{LW}] \tag{8}$$

As the columns of R_W^L are orthogonal to each other, according to Equation (8) we derive:

$$R_W^L = [Z_1 \quad Z_2 \quad Z_1 \times Z_2]^T \tag{9}$$

where Z_i represents the i-th column of Z. In Equation (8) we note that $Z_3 = -(R_W^L)^{-1}\,{}^{L}T_{LW}$, which can be re-written as:

$${}^{L}T_{LW} = -R_W^L Z_3 = [Z_1 \quad Z_2 \quad Z_1 \times Z_2]^T\, Z_3 \tag{10}$$

Thus, by solving the combination of Equations (9) and (10), R_W^L and ${}^{L}T_{LW}$ can be obtained.

Step 2: Nonlinear solution. The linear solution can be calculated using the LS method to minimise the algebraic distance between the laser scanning points and the calibration plane. In order to eliminate the difference between the measuring distance and algebraic distance, the nonlinear solution is employed.

In Equation (5) there are two types of distances, that is, the algebraic distance d between the calibration plane and the $\{W\}$ frame and the measured distance ${}^{W}r \cdot (R_W^L)^{-1}({}^{L}P - {}^{L}T_{LW})$. The differences of these two distances represent the distance errors between the laser scanning points and the calibration plane. The goal of the nonlinear solution is to eliminate the distance errors using the following object function:

$$\arg\min_{Z} f = \arg\min_{Z} \left[\sum_{i=1}^{N} \sum_{j=1}^{M_i} \left({}^{W}r_i \cdot \left(R_W^L\right)^{-1} \left({}^{L}P_{ij} - {}^{L}T_{LW}\right) - d_i \right)^2 \right] \tag{11}$$

In this work, Equation (11) is minimised by the nonlinear LS method (Pulford, 2010). The nonlinear LS performs optimisation processing via an initial guess of R_W^L and ${}^{L}T_{LW}$ to output the optimal estimation of R_W^L and ${}^{L}T_{LW}$. Then the geometric relationships between the laser scanner and IMU can be established to complete the coordinate transformation. The IMU usually consists of three gyros and three accelerometers. The gyros can provide the changes of Euler angles, while the accelerometers can give the specific forces. After integrating the outputs of accelerometers and gyros, the rotation and translation matrix between the $\{W\}$ frame and the $\{I\}$ frame can be obtained. Defining the rotation matrix as

https://doi.org/10.1017/S037346331800084X Published online by Cambridge University Press

R_I^W and the translation vector as ${}^I T_{WI}$, a point in the $\{I\}$ frame can be projected into the $\{W\}$ frame through:

$$ {}^W P = R_I^W {}^I P + {}^I T_{WI} \tag{12}$$

where ${}^I P$ represents the point in the $\{I\}$ frame, ${}^W P$ denotes the point in the $\{W\}$ frame.

Substituting Equation (1) into Equation (12), the relationship between the $\{I\}$ frame and the $\{L\}$ frame can be expressed by Equation (13).

$$ {}^L P = R_W^L \left(R_I^W {}^I P + {}^I T_{WI} \right) + {}^L T_{LW} \tag{13}$$

2.2. *Error Modelling of LSINS.* The kinematic model of LSINS is $\dot{Y} = F(y, u)$, where $y = [{}^O T_{WO} \ {}^O V \ \Theta]^T$ is the state vector and u is the input parameter. The LSINS kinematic model can be calculated as:

$$ \begin{cases} {}^O \dot{T}_{WO} = R_O^W \cdot {}^O V \\ {}^O \dot{V} = {}^O a_O - (\Omega_{IL}^O + \Omega_{IO}^O) \cdot {}^O V \\ \dot{\Theta} = \Omega_E^{-I} \cdot {}^O \omega_{WO} \end{cases} \tag{14}$$

where ${}^O \dot{T}_{WO}$ denotes the translation vector from the $\{W\}$ frame origin to the $\{O\}$ frame origin; ${}^O V$ represents the velocity of the moving object in the $\{O\}$ frame; $\Theta = [\alpha \ \beta \ \theta]$ denotes the roll, pitch and yaw of the moving object; R_O^W represents the rotation matrix from the $\{O\}$ frame to the $\{W\}$ frame; ${}^O a_O = f^O + g^O$ is the moving object's acceleration in the $\{O\}$ frame, f^O and g^O denote the specific force and local gravity vectors of the object in the $\{O\}$ frame, respectively, and ${}^O \omega_{WO}$ denotes the angle rate of the origin of the $\{O\}$ frame to the $\{W\}$ frame. Ω_E^{-1} can be defined as:

$$ \Omega_E^{-1} = \begin{bmatrix} 1 & \sin\alpha \tan\beta & \sin\alpha \tan\beta \\ 0 & \cos\alpha & -\sin\alpha \\ 0 & \sin\alpha / \cos\beta & \cos\alpha / \cos\beta \end{bmatrix} \tag{15}$$

where α and β are the roll and pitch angle of the moving object.

The standard form of localisation equations can be expressed as $\hat{B} = F(\hat{b}, \hat{u})$, where $\hat{B}$ is the estimated value of the state $\hat{b}$, and $\hat{u}$ is the measured input. The localisation equations of LSINS can be calculated as (Huang, 2010):

$$ \begin{cases} {}^O \dot{\hat{T}}_{WO} = \hat{R}_O^W \cdot {}^O \hat{V} \\ {}^O \dot{\hat{V}} = {}^O \hat{a}_O - (\hat{\Omega}_{IL}^O + \hat{\Omega}_{IO}^O) \cdot {}^O \hat{V} \\ \dot{\hat{\Theta}} = \hat{\Omega}_E^{-I} \cdot {}^O \hat{\omega}_{WO} \end{cases} \tag{16}$$

where ${}^O \hat{\omega}_{WO} = {}^O \hat{\omega}_{IO} - {}^O \hat{\omega}_{IW}$, ${}^O \hat{\omega}_{IW} = \hat{R}_W^O \cdot {}^W \hat{\omega}_{LW}$ with ${}^W \hat{\omega}_{LW} = \omega_{IL} [\cos\hat{\alpha} \ \ 0 \ \ -\sin\hat{\alpha}]$ and $\hat{\alpha}$ is the measured attitude. ${}^O \hat{a}_O$ is computed as:

$$ {}^O \hat{a}_O = f^O + g^O + \gamma_a + b_a \tag{17}$$

where γ_a is the measurement noise with Gaussian distribution and b_a is the random noise.

https://doi.org/10.1017/S037346331800084X Published online by Cambridge University Press

The error state vector includes the position velocity and attitude errors.

(1) The position errors: the errors of position are computed as:

$$\delta({}^{W}\dot{T}_{WO}) = R_O^W \cdot {}^{O}V - \hat{R}_O^W \cdot {}^{O}\hat{V} = \hat{R}_O^W \cdot \delta({}^{O}V) - {}^{W}\hat{V} \cdot \rho \tag{18}$$

where $R_O^W = \hat{R}_O^W(I + \rho)$, $I = (R_W^L)^T \cdot R_W^L$, ρ is the tilt error of the calibration plane, and ${}^{O}V = {}^{O}\hat{V} + \delta({}^{O}V)$.

(2) The velocity errors: the errors of velocity can be calculated as:

$$\begin{aligned}\delta({}^{O}\dot{V}) &= {}^{O}\dot{V} - {}^{O}\dot{\hat{V}} = {}^{O}a_O - (\Omega_{IL}^O + \Omega_{IO}^O) \cdot {}^{O}V - {}^{O}\hat{a}_O + (\hat{\Omega}_{IL}^O + \hat{\Omega}_{IO}^O) \cdot {}^{O}\hat{V} \\ &= \hat{R}_O^W \left(\left(\frac{\partial \left(g^W\right)}{\partial \left({}^{W}T_{WO}\right)} + {}^{W}\hat{V} \cdot \frac{\partial \left({}^{W}\omega_{IL}\right)}{\partial \left({}^{W}T_{WO}\right)} \right) \delta \left({}^{W}T_{WO}\right) \right. \\ &\quad \left. + \left(g^W + {}^{W}\omega_{IL} \left({}^{W}\hat{V}\right)^T - \left({}^{W}\omega_{IL}\right)^T \cdot {}^{W}\hat{V} \cdot I \right) \rho \right) \\ &\quad - (\hat{\Omega}_{IL}^O + \hat{\Omega}_{IO}^O)\delta({}^{O}V) - \delta b_a - {}^{O}\hat{V} \cdot \delta b_g - \gamma_a - {}^{O}\hat{V} \cdot \gamma_g \end{aligned} \tag{19}$$

where g^W represents the local gravity vector of the moving object in the $\{W\}$ frame, b_g is the gyro bias due to random plus noise, γ_g represents the white Gaussian measuring noise and ${}^{W}\omega_{IL}$ in the $\{W\}$ frame represents the angular rate from the origin of the $\{L\}$ frame to the $\{I\}$ frame.

(3) The attitude errors: the attitude error is given in Equation (20):

$$\delta(\dot{\Theta}) = \dot{\Theta} - \dot{\hat{\Theta}} = \Omega_E^{-1} \cdot {}^{W}\hat{\omega}_{IW} - \delta({}^{W}\omega_{IW}) - \hat{R}_I^W(\delta b_g + \gamma_g) \tag{20}$$

where $\delta({}^{W}\omega_{IW})$ is computed as:

$$\delta({}^{W}\omega_{IW}) = -\omega_{IL} \cdot \begin{bmatrix} \sin\alpha \\ 0 \\ \cos\alpha \end{bmatrix} \cdot \frac{\partial\Theta}{\partial({}^{W}R_{IW})} \cdot \delta({}^{W}R_{IW}) \tag{21}$$

The error state vector can be expressed as a function of the position velocity and attitude errors in Equation (22):

$$\begin{cases} x = [\delta({}^{W}T_{WO}) \quad \delta({}^{O}V) \quad \delta\Theta \quad \delta b_a \quad \delta b_g]^T \\ b = [b_a \quad b_g]^T \\ \gamma = [\gamma_a \quad \gamma_g]^T \end{cases} \tag{22}$$

where x, γ and b denote the error state vector, measuring noise vector and process noise vector.

https://doi.org/10.1017/S037346331800084X Published online by Cambridge University Press

Based on Equations (18), (19), (20) and (22), the measurement error model of LSINS is obtained as:

$$\begin{bmatrix} \delta({}^{W}\dot{T}_{WO}) \\ \delta({}^{O}\dot{V}) \\ \delta\dot{\Theta} \\ \delta\dot{\omega}_{ba} \\ \delta\dot{\omega}_{bg} \end{bmatrix} = \begin{bmatrix} \hat{R}_O^W \frac{\partial(g^W)}{\partial({}^{W}T_{WO})} & \hat{R}_O^W & -{}^{W}\hat{V} & 0 & 0 \\ 0 & -\left(\hat{\Omega}_{IL}^{O} + \hat{\Omega}_{IO}^{O}\right) & -\hat{R}_O^W g^W & -I & -{}^{O}\hat{V} \\ 0 & 0 & \hat{\Omega}_E^{-1} & 0 & -\hat{R}_O^W \\ 0 & 0 & 0 & 0 & 0 \\ 0 & 0 & 0 & 0 & 0 \end{bmatrix} \cdot \begin{bmatrix} \delta({}^{W}T_{WO}) \\ \delta({}^{o}V) \\ \delta\Theta \\ \delta\omega_{ba} \\ \delta\omega_{bg} \end{bmatrix} + \begin{bmatrix} -I & 0 & 0 & 0 \\ 0 & -{}^{O}\hat{V} & 0 & 0 \\ 0 & -\hat{R}_O^W & 0 & 0 \\ 0 & 0 & I & 0 \\ 0 & 0 & 0 & I \end{bmatrix} \cdot \begin{bmatrix} \gamma_a \\ \gamma_g \\ b_a \\ b_g \end{bmatrix} \tag{23}$$

2.3. *LSINS Navigation Processing.* In the LSINS aided navigation process, the IMU can be applied to measure the position and orientation of moving objects, while the laser scanner can provide accurate distance and azimuth information to a landmark. SVDUKF can be used to combine the IMU and the laser scanner to predict the position of moving objects. The observation functions of SVDUKF are given by Equation (24):

$$X_k = \begin{bmatrix} p_{IMU}^n - p_{LiDAR}^n \\ \varepsilon_{IMU}^n - \varepsilon_{LiDAR}^n \end{bmatrix} = H_k x_k + b_k + \gamma_k \tag{24}$$

where X_k is a measurement vector of LSINS, p_{IMU}^n is the predicted position from the IMU mechanisation, p_{LiDAR}^n is the observed position from LiDAR and ε_{IMU}^n and ε_{LiDAR}^n are the predicted and observed angles, respectively. The LiDAR observed angle can be obtained from LiDAR scan matching. H_k is the designed matrix that describes the relationship between the state vector and the measurement vector of LSINS.

The LSINS navigation process can be carried out as the following two steps. The first step is time propagation, which aims to integrate the outputs of the IMU and to obtain the estimations of current states. The second step is measurements updating. The laser scanner measurements are used to correct the states estimations in step 1.

Step 1: Time propagation.

(1) In time t_k, obtain X_k^+ and P_k^+ from the IMU, and incorporate into $\dot{X} = f(X, u)$ over $t \in (t_k, t_{k+1})$ to get X_{k+1}^-.
(2) Calculate $P_{k+1}^- = \Phi P_k^+ \Phi^T + Q_d$, where $Q_d = GQG^T T$, $T = t_{k+1} - t_k$ and $\Phi = e^{HT}$ with $\|HT\| \ll 1$.

Step 2: Measurement updating.

(1) In time t_k predict $Y_{k+1}^- = h(X_{k+1}^-)$.
(2) The measurement residual is $\delta Y_{k+1} = Y_{k+1} - Y_{k+1}^-$.

https://doi.org/10.1017/S037346331800084X Published online by Cambridge University Press

(3) The correction gain is $K_{k+1} = P_{k+1}^{-} H_{k+1}^{T} (H_{k+1} P_{k+1}^{-} H_{k+1}^{T} + R_{k+1})^{-1}$.
(4) Correct the state $X_{k+1}^{+} = X_{k+1}^{-} + \delta Y_{k+1} K_{k+1}$.
(5) Update the error covariance $P_{k+1}^{+} = K_{k+1} R_{k+1} K_{k+1}^{T} + (I - K_{k+1} H_{k+1}) P_{k+1}^{+} (I - K_{k+1} H_{k+1})^{-1}$.

3. OPTIMAL ESTIMATION USING RBF-IMPROVED SVDUKF.

After the error state vector and error measurement model of LSINS are established, the optimal estimation procedure of RBF-improved SVDUKF is conducted to improve the position accuracy of LSINS.

3.1. *SVDUKF algorithm.*

Assume that the error state vector and the error measurement equation of LSINS are of discrete-time nonlinear systems:

$$\begin{cases} x_{t+1} = f(x_t) + b_t \\ y_t = h(x_t) + \gamma_t \end{cases} \tag{25}$$

where $f(\cdot)$ is the nonlinear error state updating function and $h(\cdot)$ is the error measurement function. The estimation procedure of SVDUKF includes the following four steps:

(1) Initialisation:

$$\begin{cases} \hat{x}_0 = E[x_0] \\ S_0 = E[(x_0 - \hat{x}_0)(x_0 - \hat{x}_0)^T] \end{cases} \tag{26}$$

(2) Calculate the sigma points with corresponding weight coefficients:

$$\begin{cases} S_{t-1} = U_{t-1} \cdot \Lambda_{t-1} \cdot C_{t-1}^{T} = U_{t-1} \cdot \begin{bmatrix} G_{t-1} & 0 \\ 0 & 0 \end{bmatrix} \cdot C_{t-1}^{T} \\ \chi_{i,t-1} = \hat{x}_{t-1} + (U_{t-1} \sqrt{\Lambda_{t-1}(m+\lambda)})_i, (i = 1, \ldots, m) \\ \chi_{i,t-1} = \hat{x}_{t-1} - (U_{t-1} \sqrt{\Lambda_{t-1}(m+\lambda)})_{i-m}, (i = m+1, \ldots, 2m) \\ W_0^m = \dfrac{\lambda}{m+\lambda} \\ W_0^c = \dfrac{\lambda}{m+\lambda} + 1 + \varepsilon^2 - \eta \\ W_i^m = W_i^c = \dfrac{\lambda}{2(m+\lambda)}, (i = 1, \ldots, 2m) \end{cases} \tag{27}$$

where S_{t-1} is the covariance matrix of the state vector; χ is a matrix of state sigma points; Λ_{t-1} is a diagonal fading factor matrix; $G_{t-1} = diag(g_1, g_2, \cdots, g_r)$, $g_1 \geq g_2 \geq \cdots \geq g_r \geq 0$, $g_1, g_2, \cdots, g_r$ is the singular value of S_{t-1}; r is the rank of S_{t-1}; $\chi_{t-1} \in R^{m \times (2m+1)}$ is a matrix of state sigma points; U_{t-1} and C_{t-1}^{T} are the left and right singular vectors of S_{t-1}, respectively; $\lambda = \varepsilon^2 (m + k) - m$ is a scaling parameter; $\varepsilon (0 \leq \varepsilon \leq 0{\cdot}5)$ is the pre-setting distance between the sigma point and S_{t-1}, determining the spread rate of the sigma points around the mean of state x; k is a secondary scaling parameter, which is usually set to $3 - m$ and η denotes the prior knowledge of the distribution of x.

https://doi.org/10.1017/S037346331800084X Published online by Cambridge University Press

(3) Time updating equation:

$$\begin{cases} \chi_{t|t-1} = f(\chi_{t-1}) \\ \hat{x}_{t|t-1} = \sum_{i=0}^{2m} W_i^m \chi_{i,t|t-1} \\ S_{t|t-1} = \sum_{i=0}^{2m} W_i^c (\chi_{i,t|t-1} - \hat{x}_{t|t-1}) \cdot (\chi_{i,t|t-1} - \hat{x}_{t|t-1})^T + b_t \\ y_{t|t-1} = h(\chi_{t|t-1}) \\ \hat{y}_{t|t-1} = \sum_{i=0}^{2m} W_i^m y_{i,t|t-1} \end{cases} \tag{28}$$

where $\hat{x}_{t|t-1}$ is the predicted state value and $S_{t|t-1}$ is the predicted covariance matrix of the state vector.

(4) Error measurement updating equations:

$$\begin{cases} S_{y_t y_t} = \sigma_i \sum_{i=0}^{2m} W_i^c (y_{i,t|t-1} - \hat{y}_{t|t-1}) \cdot (y_{i,t|t-1} - \hat{y}_{t|t-1})^T + \gamma_t \\ S_{x_t y_t} = \sigma_i \sum_{i=0}^{2m} W_i^c (\chi_{i,t|t-1} - \hat{x}_{t|t-1})(y_{i,t|t-1} - \hat{y}_{t|t-1})^T \\ \kappa_t = S_{x_t y_t} \cdot S_{y_t y_t}^{-1} \\ \hat{x}_t = \hat{x}_{t|t-1} + \kappa_t (y_{i,t|t-1} - \hat{y}_{t|t-1}) \\ S_t = \sigma_i S_{t|t-1} - \kappa_t S_{y_t y_t} \kappa_t^T \\ D_t = y_{i,t|t-1} - \hat{y}_{t|t-1} \\ \sigma_i = \begin{cases} 1, (tr(D_t D_t^T) \le tr(S_{x_t y_t})) \\ \dfrac{tr(S_{x_t y_t})}{tr(D_t D_t^T)}, (tr(D_t D_t^T) \le tr(S_{x_t y_t})) \end{cases} \end{cases} \tag{29}$$

where σ_i represents the multiple fading factors and κ_t is the gain matrix.

3.2. *Optimisation using RBFNN.* According to Equation (29), to incorporate with the optimisation processes of $S_{y_t y_t}$, $S_{x_t y_t}$ and S_t, it is important to eliminate the influences of the gross errors, system errors and disturbances in measurement. RBFNN is one of the most popular intelligent computing methods, has a significant ability to approximate any non-linear function to a designed accuracy and also has the ability to eliminate the gross errors, system errors and disturbances more effectively and quickly. Therefore, this paper will adopt RBFNN to optimise $S_{y_t y_t}$, $S_{x_t y_t}$ and S_t.

Figure 2 shows the structure of a three layers RBFNN, consisting the input layer, the hidden layer and the output layer. We use $S_{y_t y_t}$, $S_{x_t y_t}$, S_t to denote the input and F_i^l to express

https://doi.org/10.1017/S037346331800084X Published online by Cambridge University Press

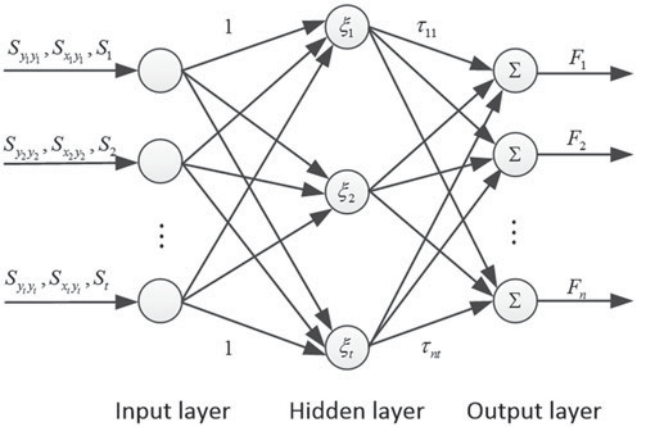

Figure 2. RBFNN architecture.

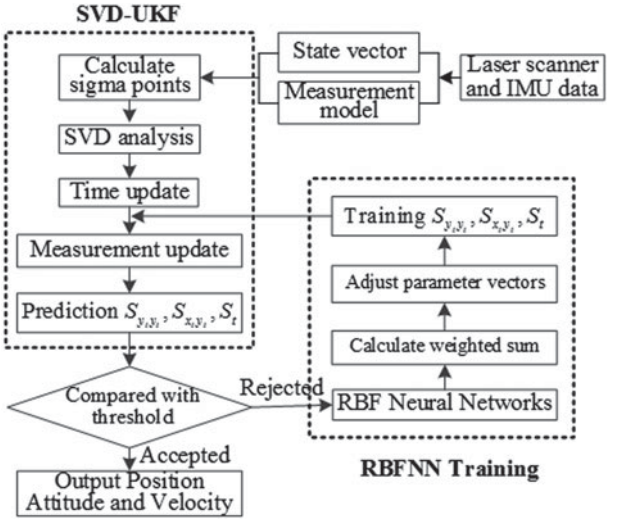

Figure 3. Flow chart of the RBFNN aiding SVDUKF procedure.

the output of the i-th node in the l-th layer. To clearly explain the signal propagation and the mathematical function in each layer, the functions of RBFNN can be represented as follows.

Input layer: Every node in the input layer corresponds to one input variable $\Gamma = S_{y_t y_t}$ or $S_{x_t y_t}$ or S_t, and transmits the input values directly to the next layer, it is written as (Liu and Li, 2017):

$$\Gamma_i^1 = F_i^1, (i = 1, 2, \cdots, t) \tag{30}$$

Hidden layer: Every node in the hidden layer corresponding to the input layer is calculated as:

$$\Gamma_i^2 = \sum_{i=1}^{t} F_i^1, (i = 1, 2, \cdots, t) \tag{31}$$

https://doi.org/10.1017/S037346331800084X Published online by Cambridge University Press

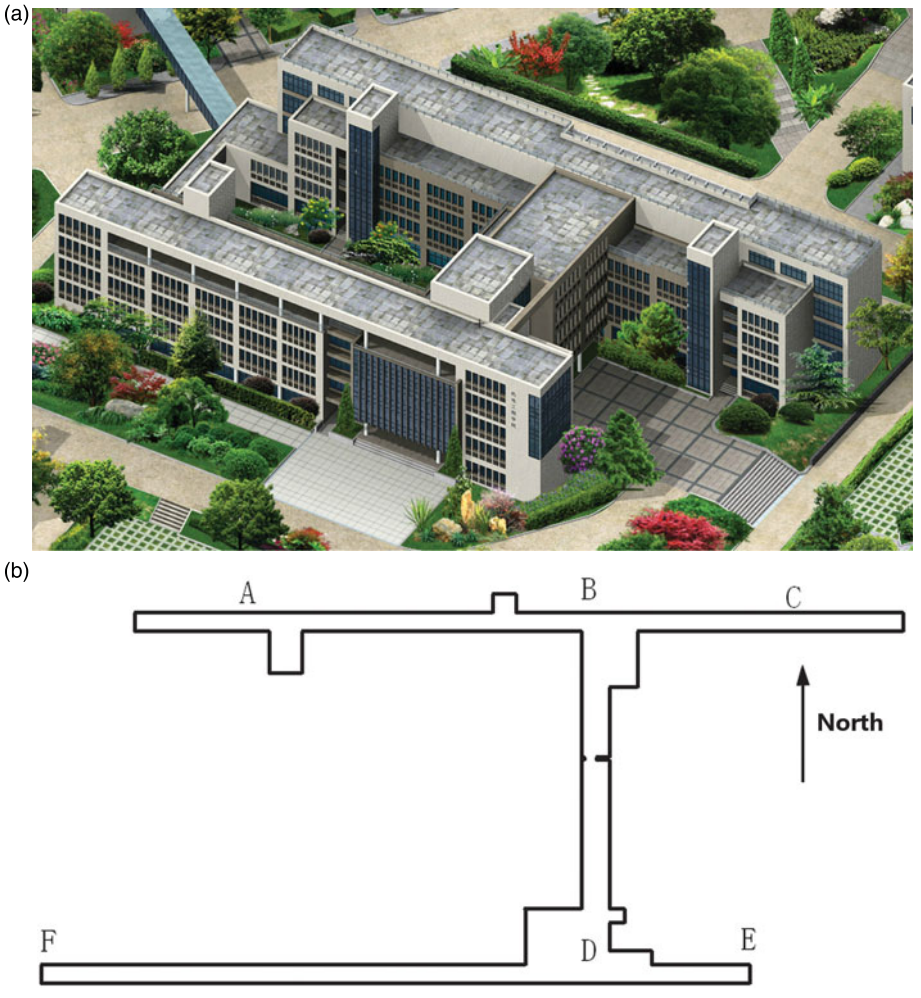

Figure 4. Experimental site: (a) 3D model of the experimental site; (b) floor map of the fourth floor.

According to the non-linear transfer function the output of each node is calculated as:

$$F_i^2 = \xi_i = \frac{1}{1 + e^{-\Gamma_i^2}}, (i = 1, 2, \cdots, t) \tag{32}$$

Output layer: Each node in the output layer connects to all output nodes of the hidden layer. The output of each node in the output layer is computed via the weighted sum:

$$\Upsilon_j = F_j^3 = \Gamma_j^3 = \sum_{j=1}^{t} O_{ij} \cdot F_j^2 = \sum_{j=1}^{t} O_{ij} \cdot \xi_j, (i = 1, 2, \cdots, n) \tag{33}$$

https://doi.org/10.1017/S037346331800084X Published online by Cambridge University Press

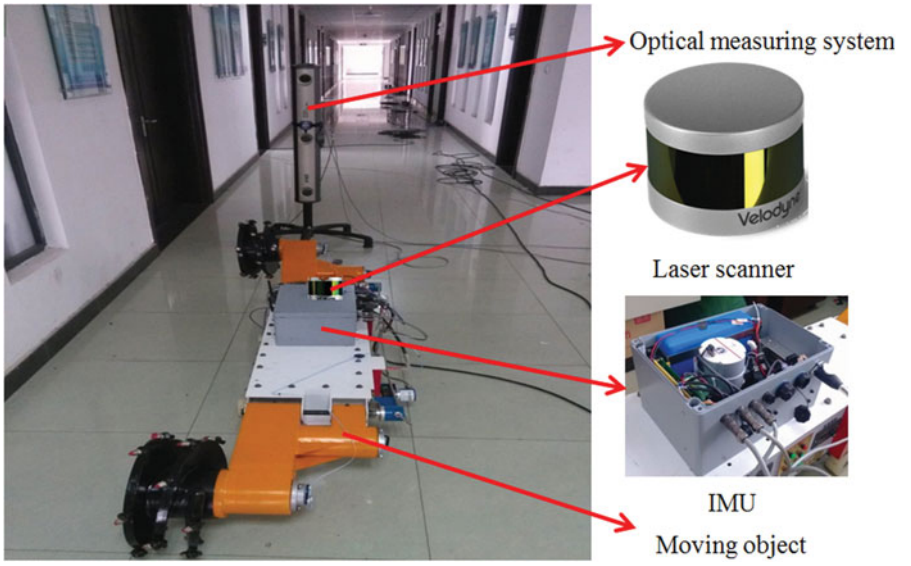

Figure 5. Experiment layouts.

The adjustable parameter vectors of O, ξ and Υ in RBFNN can be defined as follows:

$$O = \begin{bmatrix} O_{11} & O_{12} & \cdots & O_{1t} \\ O_{21} & O_{22} & \cdots & O_{2t} \\ \vdots & \vdots & \cdots & \vdots \\ O_{n1} & O_{n2} & \cdots & O_{nt} \end{bmatrix}, \xi = \begin{bmatrix} \xi_1 \\ \xi_2 \\ \vdots \\ \xi_k \end{bmatrix}, \Upsilon = \begin{bmatrix} \Upsilon_1 \\ \Upsilon_2 \\ \vdots \\ \Upsilon_n \end{bmatrix} \tag{34}$$

Thus, the output vector of RBFNN can be modified as follows:

$$\Upsilon = O^T \xi \tag{35}$$

Using the great approximation ability of RBFNN, the uncertain function H that defines an optional neural network structure is calculated as:

$$H = O^T \xi(\Gamma) + q \tag{36}$$

where $q \in R$ denotes a minimum approximation errors vector. The RBFNN approximation errors, uncertainties and other unmoulded dynamics are bounded, that is, there exists a positive constant, such as $\|q\| \leq \rho$. The corresponding estimation $\hat{F}$ can be expressed as:

$$\hat{F} = \hat{O}^T \xi(\Gamma) \tag{37}$$

where $\hat{O}$ is the tuning parameter matrix of RBFNN and it is adjusted in the learning process.

Therefore, based on Equations (27), (28), (29) and (37), the optimal estimation of LSINS can be calculated.

https://doi.org/10.1017/S037346331800084X Published online by Cambridge University Press

Table 1. The specifications of the IMU and laser scanner.

	Performance parameters	Accuracy
IMU	Horizontal Position Accuracy	0·5 m
	Vertical Position Accuracy	0·8 m
	Roll & Pitch Accuracy	0·01°
	Heading Accuracy	0·05°
	Bias Instability	0·05°/hr
	Output Data Rate	100 Hz
Laser scanner	Range accuracy	±3 cm
	Vertical FOV	30°
	Horizontal FOV	360°
	Measuring range	100 m
	Output Data Rate	300,000 pts/sec

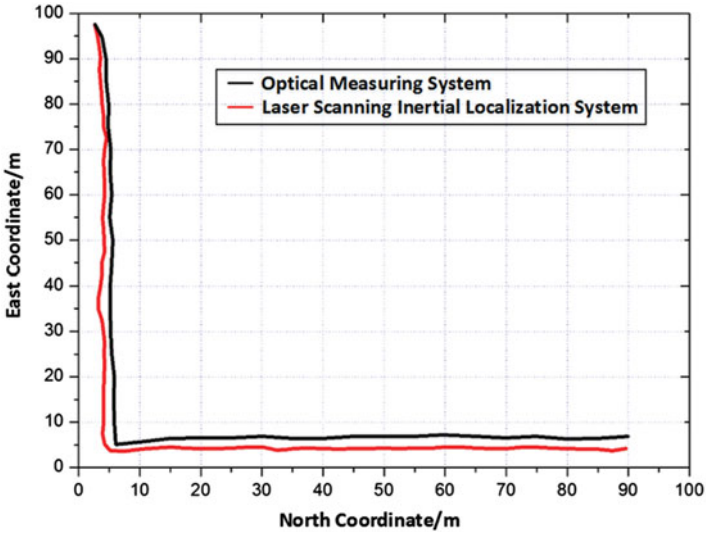

Figure 6. The measured trajectory using LSINS and optical measuring system.

3.3. *Implementation of the RBFNN aiding SVDUKF procedure.* As shown in Figure 3, the RBF-SVDUKF procedure (see Appendix) can be implemented using the following steps.

Step 1: Based on the established errors state vector and error measurement model, calculate the sigma points at time step t, and carry out SVD analysis on the obtained sigma points.

Step 2: Update the measurements of the sigma points, predict the matrix of $S_{y_t y_t}$, $S_{x_t y_t}$ and S_t and compare the predictions with the threshold (1% in this study is satisfactory). If satisfactory, output the position and attitude of the system; otherwise, go to the RBFNN optimisation procedure in Step 3.

Step 3: Implement the RBFNN training procedure to optimise $S_{y_t y_t}$, $S_{x_t y_t}$ and S_t. Repeat Step 2 and Step 3 until the threshold requirement is met.

https://doi.org/10.1017/S037346331800084X Published online by Cambridge University Press

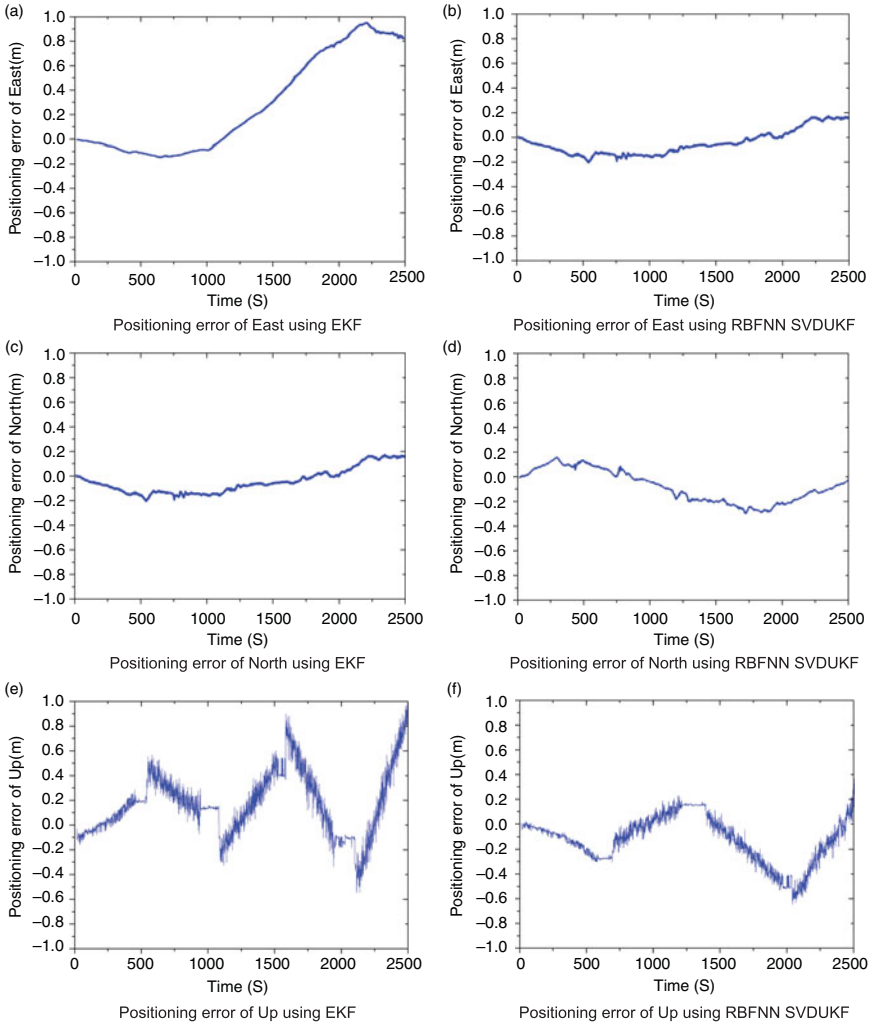

Figure 7. The positioning error using EKF and RBFNN aiding SVDUKF algorithm.

4. EXPERIMENTS AND DISCUSSION. To evaluate the effectiveness of the proposed method, field experiments were carried out at the floor of a building in the China University of Mining and Technology (see Figure 4). Figure 5 shows the experiment layouts. The experiments were conducted with a VLP-16 laser scanner and a Spatial Fibre Optic Gyro (FOG) IMU. The specifications of the IMU and laser scanner are given in Table 1.

As shown in Figure 5, we conducted the experiments in a GNSS-denied indoor environment. The total length of LSINS trajectory was 100 m and the 3D trajectory was covered in the fourth floor of the building. The LSINS was driven along the hallway of the building to evaluate the position precision. The position ground-truth values were provided by the optical measuring system, which can measure the position of LSINS with an accuracy level up to 0·1 mm. A software platform programmed with C++ was designed to record and process the raw data.

https://doi.org/10.1017/S037346331800084X Published online by Cambridge University Press

During the experiments, the proposed algorithm was evaluated from starting point to destination point along a trajectory 100 m in length. Figure 6 shows the original measurements of the LSINS (red line) and the optical measuring system (black line). As can be seen in the figure, a significant error was observed between the ground-truth and the LSINS navigation without the filter processing.

Figures 7(a), 7(c) and 7(e) show the positioning errors in the east, north and up coordinate directions using the EKF method and Figures 7(b), 7(d) and 7(f) show the positioning errors using the proposed RBF-SVDUKF method. The Root Mean Square (RMS) of the navigation errors using EKF were 0·076 m/s, 0·126 m/s and 0·275 m/s in the east, north and up directions, respectively. However, the RMS using the proposed method was 0·026 m/s, 0·047 m/s and 0·095 m/s in the three directions, respectively. The experimental results demonstrate that the position accuracy of the proposed method was improved by 23·6% compared with that of the EKF method.

As mentioned above, the proposed RBF-SVDUKF method achieved significant improvement compared with the EKF in terms of position accuracy, reliability and accumulated error. As a result, the proposed method has great potential in practical navigation in GNSS-denied environments.

5. CONCLUSIONS. In order to effectively extract and integrate the measurements from inertial sensors and laser scanners, an optimal estimation algorithm is proposed based on RBF-improved SVDUKF. The coordinate transformation between laser scanner frame and inertial sensor frame was established to model the state vector and measurement errors in LSINS. The error estimation optimisation procedure using RBF-SVDUKF was applied to improve the position accuracy of LSINS. Experimental tests were conducted to evaluate the performance of the proposed method. The analysis results demonstrate that the localisation accuracy of the proposed method has been improved by 23·6% when compared with that using the EKF method. Future research will focus on improving the calculation efficiency of the proposed RBF-SVDUKF for practical applications. We also plan to explore applications of the proposed RBF-SVDUKF in other types of multi-sensor data fusion problems.

ACKNOWLEDGEMENTS

This project was supported by National Key R&D Program of China (2018YFC0604503), the National Natural Science Foundation of Jiangsu Province (BK20150202), the National Natural Science Foundation of China (U1610251) and the Priority Academic Program Development (PAPD) of Jiangsu Higher Education Institutions. The authors would like to express their sincere thanks to them.

REFERENCES

Aghili, F. and Su, C.-Y. (2016). Robust Relative Navigation by Integration of ICP and Adaptive Kalman Filter Using Laser Scanner and IMU. *IEEE/ASME Transactions on Mechatronics*, **21**(4), 2015–2026.

Allotta, B., Costanzi, R., Meli, E., Pugi, L., Ridolfi, A. and Vettori, G. (2014). Cooperative localization of a team of AUVs by a tetrahedral configuration. *Robotics and Autonomous Systems*, **62**(8), 1228–1237.

Allotta, B., Pugi, L., Ridolfi, A., Malvezzi, M., Vettori, G. and Rindi, A. (2012). Evaluation of odometry algorithm performances using a railway vehicle dynamic model. *Vehicle System Dynamics*, **50**(5), 699–724.

Baglietto, M., Sgorbissa, A., Verda, D. and Zaccaria, R. (2011). Human navigation and mapping with a 6DOF IMU and a laser scanner. *Robotics and Autonomous Systems*, **59**(12), 1060–1069.

Bosse, M., Zlot, R. and Flick, P. (2012). Zebedee: Design of a spring-mounted 3-D range sensor with application to mobile mapping. *IEEE Transactions on Robotics*, **28**(5), 1104–1119.

Chen, G., Meng, X., Wang, Y., Zhang, Y., Tian, P. and Yang, H. (2015). Integrated WiFi/PDR/smartphone using an unscented Kalman filter algorithm for 3D indoor localization. *Sensors*, **15**(9), 24595–24614

Deng, Z.H. and Zhang, Y.Q. (2013). AN improved RBF neural network model based on hybrid learning algorithm. *Advanced Materials Research*, **718**, 2202–2207.

Gao, S.S., Wang, J.C. and Jiao, Y.L. (2010). Adaptive SVD-UKF algorithm and application to integrated navigation. *Journal of Chinese Inertial Technology*, **18**(6), 737–742.

Hesch, J.A., Kottas, D.G., Bowman, S.L. and Roumeliotis, S.I. (2016a). Consistency Analysis and Improvement of Vision-aided Inertial Navigation. *IEEE Transactions on Robotics*, **30**(1), 158–176.

Hesch, J.A., Mirzaei, F.M., Mariottini, G.L. and Roumeliotis, S.I. (2016b). A Laser-Aided Inertial Navigation System (L-INS) for human localization in unknown indoor environments. *IEEE International Conference on Robotics and Automation*, 5376–5382.

Huang, L. (2010). *LIDAR, Camera and Inertial Sensors Based Navigation Techniques for Advanced Intelligent Transportation Systems*. *Ph.D. dissertation*, University of California, California, USA.

Jwo, D.-J. and Huang, H.-C. (2004). Neural Network Aided Adaptive Extended Kalman Filtering Approach for DGPS Positioning. *The Journal of Navigation*, **57**(3), 449–463.

Kim, H.-S., Baeg, S.-H., Yang, K.-W., Cho, K. and Park, S. (2012). An enhanced inertial navigation system based on a low-cost IMU and laser scanner. *Proceedings of SPIE - The International Society for Optical Engineering*, **8387**, 1–10.

Kong, J., Mao, X. and Li, S. (2016). BDS/GPS dual systems positioning based on the modified SR-UKF algorithm. *Sensors*, **16**(5), 1–15.

Lauterbach, H.A., Borrmann, D., He, R., Eck, D., Schilling, K. and Nüchter, A. (2015). Evaluation of a backpack-mounted 3D mobile scanning system. *Evaluation of a backpack-mounted 3D mobile scanning system*, **7**(10), 13753–13781.

Lehtola, V.V., Virtane, J.-P., Vaaja, M.T., Hyyppä, H. and Nüchter, A. (2016). Localization of a mobile laser scanner via dimensional reduction. *ISPRS Journal of Photogrammetry and Remote Sensing*, **121**, 48–59.

Liu, W. (2017). LiDAR-IMU Time Delay Calibration Based on Iterative Closest Point and Iterated Sigma Point Kalman Filter. *Sensors*, **17**, 539.

Liu, W.L. and Li, Y.W. (2017). A novel method for improving the accuracy of coordinate transformation in multiple measurement systems. *Measurement Science & Technology*, **28**(9), 095002.

Liu, W.L., Wang, Z., Wang, S. and Li, X. (2013). Error Correction for Laser Tracking System Using Dynamic Weighting Model. *Advances in Mechanical Engineering*, **5**(3), 869406.

Ma, Y., Li, Z., Malekian, R., Zhang, R., Song, X. and Sotelo, M. (2018). Hierarchical fuzzy logic-based variable structure control for vehicles platooning. *IEEE Transactions on Intelligent Transportation Systems*, **99**, 1–12.

Markham, A., Niki Trigoni, N., Macdonald, D.W. and Ellwood, S.A. (2012). Underground Localization in 3-D Using Magneto-Inductive Tracking. *IEEE Sensors Journal*, **12**(6), 1809–1816.

Pulford, G.W. (2010). Analysis of a nonlinear least squares procedure used in global positioning systems. *IEEE Transactions on Signal Processing*, **58**(9), 4526–4534.

Shi, Y., Ji, S., Shao, X., Yang, P., Wu, W., Shi, Z. and Shibasaki, R. (2015). Fusion of a panoramic camera and 2D laser scanner data for constrained bundle adjustment in GPS-denied environments. *Image and Vision Computing*, **40**, 28–37.

Soloviev, A. and Uijt De Haag, M. (2010). Monitoring of moving features in laser scanner-based navigation. *IEEE Transactions on Aerospace and Electronic Systems*, **46**(4), 1699–1715.

Sun, T., Chu, H., Zhang, B., Jia, H., Guo, L., Zhang, Y. and Zhang, M. (2015). Line-of-Sight Rate Estimation Based on UKF for Strapdown Seeker. *Mathematical Problems in Engineering*, **2015**(1), 1–14.

Tan, X., Wang, J., Jin, S. and Meng, X. (2015). GA-SVR and Pseudo-position-aided GPS/INS Integration during GPS Outage. *The Journal of Navigation*, **68**(4), 678–696.

Tang, J., Chen, Y., Niu, X., Wang, L., Chen, L., Liu, J., Shi, C. and Hyyppä, J. (2015). LiDAR scan matching aided inertial navigation system in GNSS-denied environments. *Sensors*, **15**(7), 16710–16728.

Wang, J., Hu, A., Liu, C. and Li, X. (2015). A floor-map-aided WiFi/pseudo-odometry integration algorithm for an indoor positioning system. *Sensors*, **15**(4), 7096–7124.

Wu, Q., Jia, Q., Shan, J. and Meng, X. (2014). Angular velocity estimation based on adaptive simplified spherical simplex unscented Kalman filter in GFSINS, *Proceedings of the Institution of Mechanical Engineers, Part G: Journal of Aerospace Engineering*, **228**(8), 1375–1388.

Xiong, C., Han, D. and Xiong, Y. (2009). An integrated localization system for robots in underground environments. *Industrial Robot*, **36**(3), 221–229.

Zhan, R. and Wan, J. (2006). Neural network-aided adaptive unscented Kalman filter for nonlinear state estimation. *IEEE Signal Processing Letters*, **13**(7), 445–448.

APPENDIX: RBFNN AIDING SVDUKF ALGORITHM

Input: the state parameter (position, velocity and attitude measured by IMU and laser scanner) initialization error state vector and measurement model of LSINS (see Equation (19) and Equation (20))

Initialization $\hat{x}_0$ and S_0 (see Equation (22))
Calculate the sigma points χ (see Equation (23))
Update $\hat{x}_{t|t-1}$ and $S_{t|t-1}$ (see Equation (24))
Predicted S_t (see Equation (25))
while $S_t \neq$old S_t
if $\delta S_t \neq 0{\cdot}01$ then
update $S_{y_t y_t}$, $S_{x_t y_t}$
output state parameters
else
set to RBFNN procedure
training $S_{y_t y_t}$, $S_{x_t y_t}$ and S_t
check δS_t
end if
update $S_{y_t y_t}$, $S_{x_t y_t}$
output state parameters
end while

https://doi.org/10.1017/S037346331800084X Published online by Cambridge University Press